Metal Halide Perovskite Solar Module Encapsulation Using Polyolefin Elastomers: The Role of Morphology in Preventing Delamination

Haoyang Jiao,[1] Maruti Hegde,[1] Nengxu Li,[1] Michael Owen-Bellini,[2] Laura Schelhas,[2] Theo J. Dingemans,[1] and Jinsong Huang[1,3,*]

[1] *Department of Applied Physical Sciences, The University of North Carolina at Chapel Hill, Chapel Hill, North Carolina, 27599, USA*

[2] *National Renewable Energy Laboratory, Golden, Colorado, 80401, USA*

[3] *Department of Chemistry, The University of North Carolina at Chapel Hill, Chapel Hill, North Carolina, 27599, USA*

The development of perovskite solar cells (PSCs) has ushered in a new era of solar technology, characterized by its exceptional efficiency and cost-effective production. However, the soft and fragile nature of perovskites makes module encapsulation challenging. Polyolefin elastomers (POEs) have been reported to be promising encapsulants for perovskite modules. However, little research exists on identifying criteria among different types of POEs as encapsulants. Here, two POEs with different morphologies were compared as encapsulants. The first POE crystallizes during encapsulation (crystal content ∼40%), and the resulting shrinkage or warpage leads to delamination, causing minimodule failure. In contrast, perovskite minimodules encapsulated with a mostly amorphous POE exhibited better reliability and reproducibility. The best perovskite minimodules passed the thermal cycling test for 240 cycles between −40 and 85 °C and the damp heat test for 1419 h, according to the IEC 61215 standard. This study highlights the importance of the morphology of encapsulants in achieving high-quality encapsulation.

I. INTRODUCTION

Perovskite solar cells (PSCs) have demonstrated rapid improvement in power conversion efficiency (PCE), attaining 26.1% for single junction cells and 33.9% for monolithic perovskite-silicon tandem cells [1]. Despite performance advancements, perovskite photovoltaics (PV), particularly modules, continue to face long-term durability issues, which remain the most significant hurdle to commercialization. In addition to the intrinsic stability of perovskites, encapsulation technology is critical to the module's longevity [2,3]. Encapsulation serves as a protection against environmental factors such as moisture and oxygen, and thus, the encapsulant should have a low permeability [4–9]. In addition, the encapsulating materials themselves need to have an appropriate modulus to avoid stress-related damage [10], should be processable under conditions that do not damage the perovskite solar modules during production [11–14], and must remain stable during 25–30 years operation in the field.

Glass-glass lamination technology—adapted from Si and CdTe solar cell encapsulation—that incorporates various polymer encapsulants and edge sealants are widely used to encapsulate PSCs. Compared with Si and CdTe, perovskites are more temperature sensitive and softer; therefore, the encapsulants need to provide mechanical protection without introducing stress and can be laminated at a relatively low temperature. Among the diverse polymeric materials evaluated, including ethyl vinyl acetate (EVA) [10,15–21], polyisobutylene (PIB) [22,23], polyolefin elastomer (POE) [10,16,24], Surlyn [10,15], and thermoplastic polyurethane (TPU) [16,25], each demonstrated specific advantages and limitations. Notably, EVA's high encapsulation temperature (> 140 °C) and acid byproducts during aging were detrimental to perovskite device stability [26,27]. Surlyn films, despite their superior reliability, were prone to delamination issues due to their high tensile modulus [10]. Preliminary evaluation of TPU demonstrated its commendable performance in certain scenarios, but it is relatively expensive [28]. POEs have emerged as one of the most extensively researched encapsulants [10,16,24,28]. POE exhibits low water vapor transmission rates (∼0.8 g/m² day), sufficient

---

*Contact author: jhuang@unc.edu

thermal stability (degradation occurs above 300 °C), optical transparency (∼91%) [29], and can be processed at temperatures and pressures that do not damage most of the perovskites suitable for solar cells. Moreover, POEs are relatively low cost compared to other polymers that are suitable as encapsulants. POEs are typically copolymers obtained by metallocene polymerization of ethylene-based monomers along with other alpha-olefin monomers. By tuning monomer structures and monomer functionality, polymer backbone structures and architectures, and hence, their thermomechanical and morphological properties, can be easily altered. Despite widespread use as an encapsulant material by research groups, research has not yet fully explored which POE properties are required for them to act as an encapsulant for perovskite solar cells.

Herein, we compare PSC performance for two POEs as encapsulating materials. One of them, referred to as POE-1, is commercially available from DNPsolar, a subsidiary of Dai Nippon Printing Co., Ltd., Japan. The second POE used for comparison, POE-2, is an experimental grade material. The morphological characteristics and thermal and thermomechanical behaviors of POE-1 and POE-2 were studied and used to rationalize device performance and stability following encapsulation. Specifically, the performance and durability of minimodules with the

two POEs were evaluated using accelerated stress tests (thermal cycling and damp heat), in accordance with the International Electrotechnical Commission (IEC) 61215-2:2021 module qualification tests [30]. Our work demonstrates that amorphous POEs and POEs with a low degree of crystallinity result in better encapsulation for PSCs.

II. RESULTS AND DISCUSSION

A schematic diagram of the components of an encapsulated minimodule is shown in Fig. 1(a) [29]. In our typical minimodule encapsulation procedure, desiccated PIB edge sealant was adhered to the edges of ITO glass and cover glass and worked as a moisture barrier [19]. The SnPb solder coated copper ribbons [shown as rods in Fig. 1(a)] were placed between two PIB sealants to minimize moisture penetration. Two encapsulant (POE-1 or POE-2) films were placed between the cover glass and the device to reduce the thickness mismatch between PIB and POE encapsulant films. This whole assembly was then placed in a laminator for encapsulation. The optimal pressure and temperature conditions were determined based on the characterization of both POEs. Details of the encapsulation method are provided in the Supplemental Material [33].
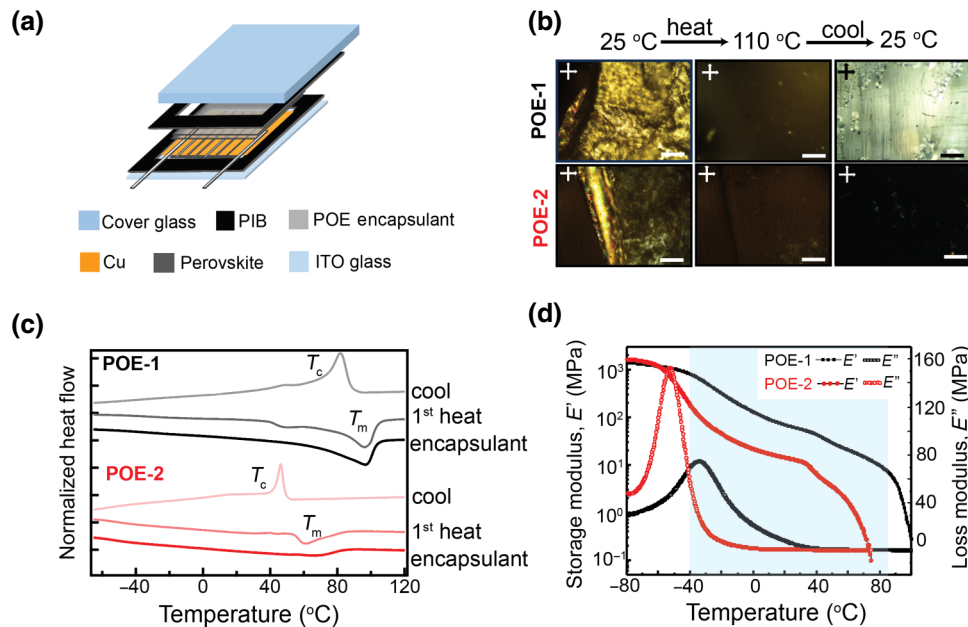

FIG. 1. PSC minimodule and POE characterization. (a) Schematic illustration of the minimodule encapsulation components. (b) Morphological changes that occur when POE-1 and POE-2 films are heated and cooled between crossed polarizers of an optical microscope. Temperatures are mentioned above the images. Scale bar in all images is 200 μm. Upon cooling, only POE-1 appears highly birefringent (high crystal content), whereas POE-2 is weakly birefringent (low crystal content). (c) DSC curves for POE-1 and POE-2 films subjected to a heating-cooling cycle. Curves are vertically translated for clarity. Analysis (heating curve) of POE films subjected to minimodule encapsulation processing conditions confirms similar thermal transitions as the first heating curves. (d) Storage (E') and loss modulus (E'') curves obtained at 1 Hz; tensile mode as a function of temperature for POE-1 and POE-2 films. Higher crystallinity in POE-1 films results in larger E' values above T_g. Blue shaded box covers the temperature range that POE encapsulants experience during thermal cycling.

Scanning thermogravimetric analysis of the two polymers (10 °C/min) revealed an onset of thermal decomposition temperature of 385 °C for both POEs [Fig. S1 within the Supplemental Material [33]], which was higher than the operational temperature range of the perovskite solar minimodules. Heating and cooling of the films on a hot stage between the crossed polarizers of an optical microscope enabled visualization of the morphological changes that occurred in the POE films during [Fig. 1(b)] minimodule encapsulation. The observed birefringence at 25 °C due to a semicrystalline morphology disappears upon complete melting at 110 °C. Upon complete melting and cooling, only POE-1 appears to be highly birefringent, i.e., POE-1 is able to recrystallize during the cooling process [Fig. 1(b), top row], whereas POE-2 stays mostly amorphous with a few scattered crystallites [Fig. 1(b), bottom row]. Additionally, the melt viscosity at 110 °C was qualitatively judged to be low enough for the processing of POEs during encapsulation. The observations from crossed polarized optical microscopy were quantitatively analyzed using differential scanning calorimetry (DSC) [Fig. 1(c)]. POE-1 exhibits a weak glass transition (T_g) that is centered at −31 °C followed by a large broad melt endotherm (T_m) (between 39 and 120 °C), with a melt enthalpy (ΔH_f) of about 90 J/g. The subsequent cooling curve reveals a large exotherm due to crystallization (T_c), with an identical ΔH of about 90 J/g. In contrast, POE-2 exhibits a lower T_g (−51 °C), with a smaller T_m peak with $\Delta H \sim 19$ J/g and crystallization upon cooling ($\Delta H = 19$ J/g). A rough estimate of the relative crystallinity value (χ_c) based on polyethylene ($\chi_{100\%} = 293$ J/g) and polypropylene ($\chi_{100\%} = 207$ J/g) indicates that χ_c for POE-1 lies between 31% and 44%, whereas χ_c for POE-2 it is between 6% and 9% [31]. These results demonstrate that POE-1 has a greater propensity to crystallize than POE-2. Thermomechanical analysis was performed on both POE films using dynamic mechanical thermal analysis [Fig. 1(d)]. At −80 °C, both films exist in a glassy state, and their stress response is dominated by the elastic component, i.e., high E' and low E'', resulting in typical glassy E' values (~1600 MPa for both POEs). Upon increasing the temperature, the polymers soften at T_g and E' decreases dramatically. Concurrently, E'' exhibits peaks at −52 and −33 °C, signifying molecular dissipative transitions, i.e., T_g at which viscoelastic behavior dominates. Although both POE-1 and POE-2 exhibit a clear rubbery plateau between 0 and 35 °C before the onset of melting, E' for POE-1 is much higher than POE-2 (at 30 °C, $E' = 62$ and 9 MPa for POE-1 and POE-2, respectively). The larger E' in the rubbery plateau region of POE-1 arises from the higher crystal content, i.e., the crystal domains act as physical cross-linking sites for the amorphous polymer chains, thereby limiting their deformation. E' drops dramatically again (onset at 45 °C for POE-1 and 35 °C for POE-2) due to crystalline

melting. The mechanical properties (Young's modulus and strength) from stress-strain measurements at 25 °C (Fig. S2 within the Supplemental Material [33]) confirm that the higher crystal content in POE-1 makes it stiffer and stronger than POE-2 above T_g.

The contrasting crystallizability of POE-1 and POE-2 impacts device encapsulation. To visualize the effect of crystallization on the dimensional stability of POE films, POE films on a Bynel™ support were subjected to the processing temperature (110 °C for 10 min) used for encapsulation followed by slow natural cooling to 25 °C. The propensity of POE-1 to crystallize significantly (between 31% and 44%) while cooling results in extensive film warping due to crystallization-induced dimensional change (warpage, shrinkage) [32] and delamination from the Bynel™ support at the edges [Fig. 2(a)]. In contrast, such extensive warpage is not observed in predominantly amorphous POE-2 films [Fig. 2(b)]. POE-2 films on a Bynel™ support remain adhered with minimal warpage due to the lack of crystallization during cooling. The estimated inward curvatures (Fig. S3 within
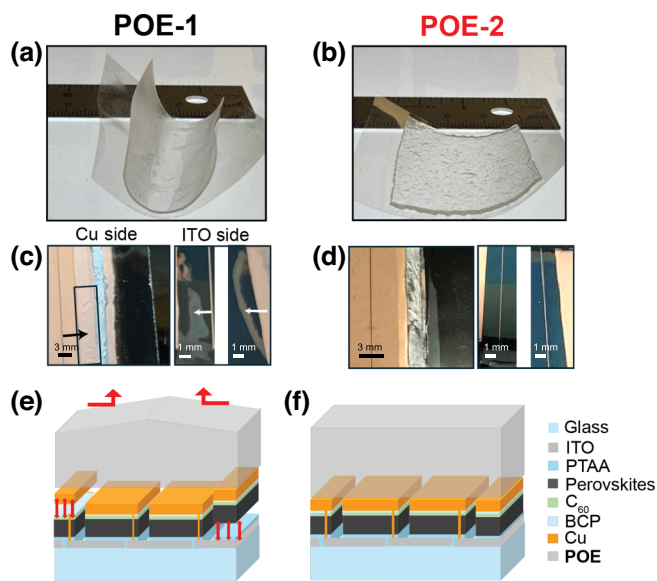

FIG. 2. Analysis of minimodules encapsulated with POE-1 and POE-2. (a) POE-1 with Bynel™ support after cooling down with warpage and delamination from the Bynel™ support at the edge. (b) POE-2 with Bynel™ support after cooling down remaining adhered with minimal warpage. (c) PSC minimodules encapsulated with POE-1; delamination of encapsulants from the device is observed predominantly at the edges on the Cu side and ITO side. Arrows point to delaminated sites. (d) PSC minimodules encapsulated with POE-1. No delamination is observed in devices encapsulated with POE-2. (e) Schematic of the POE-1 encapsulated minimodule showing the warping of POE-1 that causes delamination of Cu from the perovskite and the perovskite from the hole transporting layer (HTL). (f) Schematic of a POE-2 encapsulated minimodule without delamination issues shown for comparison.

the Supplemental Material [33]) for POE-1 are 0.75 and 2.02 cm for POE-2. A stack to mimic the minimodule was constructed by laminating PIB and POE between two glass covers and then subjecting it to the encapsulation processing conditions (Fig. S4 within the Supplemental Material [33]). The stack with POE-1 films exhibits thickness variation (5.20 mm in the center and 5.14 mm at the edge) throughout the sample due to dimensional changes (warpage, shrinkage). In contrast, the stack formed using POE-2 shows minimal thickness variations (5.36 mm in the center and 5.34 mm at the edge). The solar cell minimodules used in this work are composed of ITO/poly[bis(4-phenyl)(2,4,6-trimethylphenyl)amine] (PTAA)/formamidinium $(FA)_{0.9}Cs_{0.1}PbI_3$/C_{60}/bathocuproine (BCP)/Cu. In minimodules, crystallinity-induced dimensional changes in POE-1 caused delamination at the edges on both the Cu side and the ITO side, whereas no such issues were observed in POE-2 encapsulated minimodules [Figs. 2(c) and 2(d)]. The schematics shown in Figs. 2(e) and 2(f) help to visualize the mechanism by which delamination occurs.

Photoluminescence (PL) and electroluminescence (EL) mapping of the minimodules before and after encapsulation with POE-1 and POE-2 was performed to understand how minimodule performance was impacted by encapsulation (Fig. 3). We selected two minimodules with minimal visible delamination and optimal PCEs for this study.

The results shown in Fig. 3 are consistent with our findings shown in Fig. 2. The left edge of the minimodule postencapsulation (red and yellow framed areas marked by arrows) exhibited a clear contrast, indicating damage to the perovskite layer, which was caused by POE-1 delamination [Fig. 3(a)]. Additionally, we measured the minimodule EL with a constant injected current of 3 mA, which was about 5% of the minimodule short-circuit current to minimize possible damage to the minimodules by the forward current. We observed the disappearance of edge EL signals [Fig. 3(b)] on the POE-1 encapsulated minimodule postencapsulation. The input voltage of the minimodule during EL measurement dropped from 2.76 V (preencapsulation) to 1.62 V (postencapsulation), which indicated that the minimodule was partially short circuited or shunted at the P3 area due to the POE-1 warpage (shrinkage) at the edge [Figs. 2(e) and S4 within the Supplemental Material [33]]. In minimodules encapsulated using POE-2, there is a negligible difference in PL intensities compared to the preencapsulated minimodules [Fig. 3(c)], which means no damage to the perovskite occurs during the encapsulation process. The minimodule encapsulated with POE-2 only demonstrates a slight change in EL mapping intensities, and the measured voltage of the minimodule during EL changes slightly from 3.41 V (preencapsulation) to 3.43 V (post encapsulation), which indicates there is no big contact resistance change during encapsulation, implying superior encapsulation quality.

The PCE changes before and after lamination for both POE-1 and POE-2 encapsulated minimodules with an aperture area between 9.9 and 17.9 cm^2 are shown in Figs. S5–S7 within the Supplemental Material [33]. Since most minimodules encapsulated with POE-1 experienced delamination issues, leading to failure after lamination, only two out of eight minimodules survived with reduced V_{OC}, J_{SC}, and fill factor (FF) after lamination (Tables S1 and S2 within the Supplemental Material [33]); the surviving minimodule PCEs are shown in Fig. S5 within the Supplemental Material [33]. One of the minimodule's FF reduced from 62% to 58%, which reduced the PCE by 4.8% postencapsulation. V_{OC} of the other surviving minimodules dropped by 25.0%, I_{SC} dropped by 12.4%, and the FF dropped by 9.5%, which reduced the PCE by 40% postencapsulation. Conversely, POE-2 encapsulated minimodules demonstrated increased V_{OC} and FF, thereby enhancing the PCE (Fig. S6 within the Supplemental Material [33]). Statistical data for the performance of POE-2 encapsulated minimodules pre- and postencapsulation are shown in Fig. S7 within the Supplemental Material [33]. In total, all ten tested modules survived after POE-2 encapsulation, and detailed parameters are listed in Tables S3 and S4 within the Supplemental Material [33]. On average, the minimodules' V_{OC} increased by 2.3%, I_{SC} increased by 1.4%, FF increased by 9.3%, and the PCE increased by 12.1% postencapsulation.

Encapsulated minimodules were subjected to thermal cycling and damp heat tests. The thermal cycling test
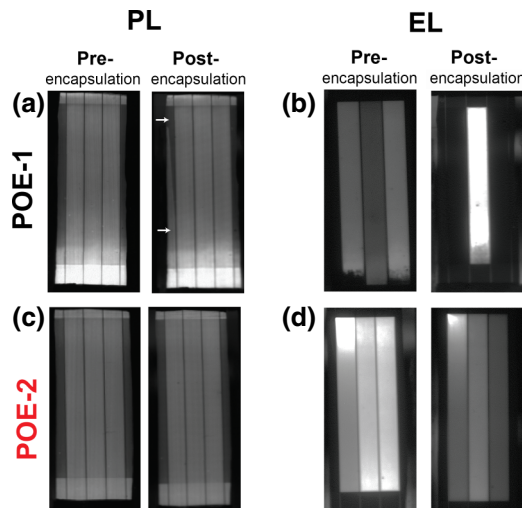

FIG. 3. PL and EL mapping of minimodules pre- and postencapsulation with POE-1 and POE-2. (a) PL of POE-1 based minimodule pre- and postencapsulation. (b) EL of POE-1 based minimodules pre- and postencapsulation. EL signals from both edges disappear postencapsulation. (c) PL of POE-2 based minimodules pre- and postencapsulation. (d) EL of POE-2-based minimodules pre- and postencapsulation.

adhered to IEC 61215 standards (200 cycles, temperature limits of -40 and $85\,°C$) and the damp heat test was performed at $85\,°C \pm 2\,°C$ at a relative humidity of 85%. While these tests do not offer a direct prediction of the device's long-term stability in field tests, they help identify reasons behind failures in the device packaging.

POE-1 encapsulated minimodules did not pass the thermal cycling test, and the edge of the minimodule showed obvious degradation [Fig. 4(a)]. In fact, the PCE of the best POE-1 encapsulated minimodule decreased by 20% of its initial PCE after only one temperature cycle [Fig. 4(b)]. Detailed parameters are listed in Table S5 within the Supplemental Material [33]. Due to the failure of the POE-1 encapsulated minimodules in the thermal cycling test, they were not subjected to subsequent damp heat testing. The best POE-2 encapsulated minimodule maintained 100% of its highest PCE after 240 thermal cycles [Fig. 4(c)]. The evolutions of V_{OC}, J_{SC}, FF, and PCE for this device are summarized in Fig. S8 within the Supplemental Material [33]. During thermal cycling, the temperature was changed between -40 and $85\,°C$, wherein E' varied between 181 and 0.1 MPa, respectively [Fig. 1(d)]. Despite this large change of stiffness, no delamination was observed during thermal cycling. Additionally, the best POE-2 encapsulated minimodule demonstrated exceptional durability, retaining 90.7% of its highest PCE after 1419 h of damp heat testing [Fig. 4(d)]. The evolutions of V_{OC}, J_{SC}, FF, and PCE for this device are summarized in Fig. S9 within the Supplemental Material [33].

III. CONCLUSIONS

The morphological, thermal, and thermomechanical characterization of two polyolefin elastomers with different crystallinity enabled the determination of how encapsulant morphology could impact PSC minimodule encapsulation. During PSC minimodule encapsulation using a highly crystallizable polymer (χ_c is between 31% and 44%), crystallization-induced warpage or shrinkage of POE-1 caused delamination and minimodule failure. In contrast, minimodules encapsulated with POE-2, which remained mostly amorphous (χ_c is only 6%–9%), not only passed the thermal cycling and damp heat tests, but also improved minimodule PCE by encapsulation. It is not clear yet why the solar cell efficiency was enhanced after encapsulation. Additionally, during thermal cycling, no delamination was observed, despite dramatic changes in POE-2 stiffness; E' ranges from 181 MPa ($-40\,°C$) to 0.1 MPa ($85\,°C$). Our work provides crucial insights for guiding encapsulant selection for enhanced minimodule stability and performance.

FIG. 4. Durability assessments of POE-1 and POE-2 encapsulated minimodules. (a) PCE change of a POE-1 encapsulated minimodule during a thermal cycling test with the final picture of the minimodule, showing the degradation of the edge perovskite. (b) J-V curves of a POE-1 encapsulated minimodule after encapsulation and one thermal cycle. (c) PCE change of POE-2 encapsulated minimodule during the thermal cycling test with the final picture of the minimodule, showing no obvious degradation. (d) PCE evolution of POE-2 encapsulated minimodule during the damp heat test with the final picture of the minimodule, showing no obvious degradation.

[1] *Best Research-Cell Efficiency Chart.* https://www.nrel.gov/pv/cell-efficiency.html (accessed 2024-02-22).

[2] S. Ma, G. Yuan, Y. Zhang, N. Yang, Y. Li, and Q. Chen, Development of encapsulation strategies towards the commercialization of perovskite solar cells, Energy Environ. Sci. **15** (1), 13 (2022).

[3] Q. Emery, M. Remec, G. Paramasivam, S. Janke, J. Dagar, C. Ulbrich, R. Schlatmann, B. Stannowski, E. Unger, and M. Khenkin, Encapsulation and outdoor testing of perovskite solar cells: Comparing industrially relevant process with a simplified lab procedure, ACS Appl. Mater. Interfaces **14** (4), 5159 (2022).

[4] T. Wang, J. Yang, Q. Cao, X. Pu, Y. Li, H. Chen, J. Zhao, Y. Zhang, X. Chen, and X. Li, Room temperature nondestructive encapsulation via self-crosslinked fluorosilicone polymer enables damp heat-stable sustainable perovskite solar cells, Nat. Commun. **14** (1), 1342 (2023).

[5] H. Wang, Y. Zhao, Z. Wang, Y. Liu, Z. Zhao, G. Xu, T.-H. Han, J.-W. Lee, C. Chen, D. Bao, Y. Huang, Y. Duan, and Y. Yang, Hermetic seal for perovskite solar cells: An improved plasma enhanced atomic layer deposition encapsulation, Nano Energy **69**, 104375 (2020).

[6] E. Y. Choi, J. Kim, S. Lim, E. Han, A. W. Y. Ho-Baillie, and N. Park, Enhancing stability for organic-inorganic perovskite solar cells by atomic layer deposited Al_2O_3 encapsulation, Sol. Energy Mater. Sol. Cells **188**, 37 (2018).

[7] H. Asgarimoghaddam, Q. Chen, F. Ye, A. Shahin, B. Song, and K. P. Musselman, Zinc aluminum oxide encapsulation layers for perovskite solar cells deposited using spatial atomic layer deposition, Small Methods **8** (3), 2300995 (2024).

[8] J. Zhou, X. Tian, Y. Gao, S. Zhang, Y. Zhang, Z. Liu, and W. Chen, Enhancing the stability of perovskite solar cells with a multilayer thin-film barrier, ACS Appl. Energy Mater. **6** (3), 1413 (2023).

[9] Y. Wang, I. Ahmad, T. Leung, J. Lin, W. Chen, F. Liu, A. M. C. Ng, Y. Zhang, and A. B. Djurišić, Encapsulation and stability testing of perovskite solar cells for real life applications, ACS Mater. Au **2** (3), 215 (2022).

[10] R. Cheacharoen, K. A. Bush, N. Rolston, D. Harwood, R. H. Dauskardt, and M. D. McGehee, in *2018 IEEE 7th World Conference on Photovoltaic Energy Conversion (WCPEC) (A Joint Conference of 45th IEEE PVSC, 28th PVSEC & 34th EU PVSEC)* (IEEE, Waikoloa Village, HI, 2018), pp. 3498–3502.

[11] M. Cao, W. Ji, C. Chao, J. Li, F. Dai, and X. Fan, Recent advances in UV-cured encapsulation for stable and durable perovskite solar cell devices, Polymers **15** (19), 3911 (2023).

[12] Y. I. Lee, N. J. Jeon, B. J. Kim, H. Shim, T. Yang, S. I. Seok, J. Seo, and S. G. Im, A low-temperature thin-film encapsulation for enhanced stability of a highly efficient perovskite solar cell, Adv. Energy Mater. **8** (9), 1701928 (2018).

[13] F. J. Ramos, T. Maindron, S. Béchu, A. Rebai, M. Frégnaux, M. Bouttemy, J. Rousset, P. Schulz, and N. Schneider, Versatile perovskite solar cell encapsulation by low-temperature ALD-Al_2O_3 with long-term stability improvement, Sustainable Energy Fuels **2** (11), 2468 (2018).

[14] A. Perrotta, C. Fuentes-Hernandez, T. M. Khan, B. Kippelen, M. Creatore, and S. Graham, Near room-temperature direct encapsulation of organic photovoltaics by plasma-based deposition techniques, J. Phys. D: Appl. Phys. **50** (2), 024003 (2017).

[15] R. Cheacharoen, N. Rolston, D. Harwood, K. A. Bush, R. H. Dauskardt, and M. D. McGehee, Design and understanding of encapsulated perovskite solar cells to withstand temperature cycling, Energy Environ. Sci. **11** (1), 144 (2018).

[16] M. D. Kempe, D. C. Miller, J. H. Wohlgemuth, S. R. Kurtz, J. M. Moseley, Q. Shah, G. Tamizhmani, K. Sakurai, M. Inoue, T. Doi, A. Masuda, S. L. Samuels, and C. E. Vanderpan, in *2012 38th IEEE Photovoltaic Specialists Conference* (IEEE, Austin, TX, 2012), pp. 001871–001876.

[17] N. Kim, C. Han, J. Lee, D. Baek, and D. Kim, in *2012 38th IEEE Photovoltaic Specialists Conference* (IEEE, Austin, TX, USA, 2012), pp. 000887–000890.

[18] C. Peike, P. Hülsmann, M. Blüml, P. Schmid, K.-A. Weiß, and M. Köhl, Impact of permeation properties and backsheet-encapsulant interactions on the reliability of PV modules, ISRN Renewable Energy **2012**, 1 (2012).

[19] M. D. Kempe, D. Panchagade, M. O. Reese, and A. A. Dameron, Modeling moisture ingress through polyisobutylene-based edge-seals, Prog. Photovoltaics **23** (5), 570 (2015).

[20] K. A. Bush, *et al.*, 23.6%-Efficient monolithic perovskite/silicon tandem solar cells with improved stability, Nat. Energy **2** (4), 17009 (2017).

[21] E. Velilla, F. Jaramillo, and I. Mora-Seró, High-throughput analysis of the ideality factor to evaluate the outdoor performance of perovskite solar minimodules, Nat. Energy **6** (1), 54 (2021).

[22] X. Wang, G. S. Huang, J. R. Wu, Y. J. Nie, X. J. He, and K. W. Xiang, Molecular motions in glass-rubber transition region in polyisobutylene investigated by two-dimensional correlation dielectric relaxation Spectroscopy, Appl. Phys. Lett. **99** (12), 121902 (2011).

[23] M. J. McEachran, J. F. Trant, I. Sran, J. R. De Bruyn, and E. R. Gillies, Carboxylic acid-functionalized butyl rubber: Synthesis, characterization, and physical properties, Ind. Eng. Chem. Res. **54** (17), 4763 (2015).

[24] J. Kapur, J. L. Norwood, and C. D. Cwalina, in *2013 IEEE 39th Photovoltaic Specialists Conference (PVSC)* (IEEE, Tampa, FL, USA, 2013), pp. 3020–3023.

[25] G. Scetta, J. Ju, N. Selles, P. Heuillet, M. Ciccotti, and C. Creton, Strain induced strengthening of soft thermoplastic polyurethanes under cyclic deformation, J. Polym. Sci. **59** (8), 685 (2021).

[26] F. Matteocci, L. Cinà, E. Lamanna, S. Cacovich, G. Divitini, P. A. Midgley, C. Ducati, and A. Di Carlo, Encapsulation for long-term stability enhancement of perovskite solar cells, Nano Energy **30**, 162 (2016).

[27] Q. Dong, F. Liu, M. K. Wong, H. W. Tam, A. B. Djurišić, A. Ng, C. Surya, W. K. Chan, and A. M. C. Ng, Encapsulation of perovskite solar cells for high humidity conditions, ChemSusChem **9** (18), 2597 (2016).

[28] Z. Fu, M. Xu, Y. Sheng, Z. Yan, J. Meng, C. Tong, D. Li, Z. Wan, Y. Ming, A. Mei, Y. Hu, Y. Rong, and H. Han, Encapsulation of printable mesoscopic perovskite solar cells enables high temperature and long-term outdoor stability, Adv. Funct. Mater. **29** (16), 1809129 (2019).

[29] R. Cheacharoen, C. C. Boyd, G. F. Burkhard, T. Leijtens, J. A. Raiford, K. A. Bush, S. F. Bent, and M. D. McGehee,

Encapsulating perovskite solar cells to withstand damp heat and thermal cycling, Sustainable Energy Fuels **2** (11), 2398 (2018).

[30] *IEC 61215-2:2021|IEC Webstore.* https://webstore.iec.ch/publication/61350 (accessed 2024-04-12).

[31] *Crystallinity/Degree of Crystallinity.* NETZSCH - Analyzing and Testing. Leading in Thermal Analysis, Rheology and Fire Testing. https://analyzing-testing.netzsch.com/en-US/training-know-how/glossary/crystallinity-degree-of-crystallinity (accessed 2024-03-14).

[32] A. Kościuszko, D. Marciniak, and D. Sykutera, Post-processing time dependence of shrinkage and mechanical properties of injection-molded polypropylene, Materials **14** (1), 22 (2021).

[33] See the Supplemental Material at http://link.aps.org/supplemental/10.1103/PRXEnergy.3.023013, which includes Ref. [34], for detailed information on device fabrication; device encapsulation procedures; and descriptions of the stress-strain measurements, dynamic mechanical thermal analysis measurements, thermogravimetric analysis, differential scanning calorimetry, cross-polarized optical microscopy, photoluminescence mapping, and electron luminescence mapping measurements.

[34] Z. Xiao, D. Wang, Q. Dong, Q. Wang, W. Wei, J. Dai, X. Zeng, and J. Huang, Unraveling the hidden function of a stabilizer in a precursor in improving hybrid perovskite film morphology for high efficiency solar cells, Energy Environ. Sci. **9** (3), 867 (2016).